DOI: 10.1002/11yp.14372

RESEARCH AND OBSERVATORY CATCHMENTS: THE LEGACY AND THE FUTURE



Check for updates

Using dissolved organic matter fluorescence to predict total mercury and methylmercury in forested headwater streams, Sleepers River, Vermont USA

James B. Shanley¹ | Vivien F. Taylor² | Kevin A. Ryan³ | Ann T. Chalmers¹ | Julia Perdrial⁴ | Aron Stubbins³

Correspondence

James B. Shanley, U.S. Geological Survey, Montpelier, Vermont 05602, USA. Email: jshanley@usgs.gov

Funding information

U.S. Geological Survey; USGS Water Resources Research Institutes 104g program

Abstract

Aqueous transport of mercury (Hg) across the landscape is closely linked to dissolved organic matter (DOM). Both quantity and quality of DOM affect Hg mobility, as well as the formation and transport of toxic methylmercury (MeHg), but only a limited number of field studies have investigated Hg and MeHg with respect to specific DOM components. We investigated these interactions at the 41-ha forested W-9 catchment at Sleepers River, Vermont, which has a long history of mercury and other biogeochemical research. We examined spatial and temporal patterns of filtered Hg fractions and dissolved organic carbon (DOC) concentration, DOM quality, and major solutes at 12 stream sites within W-9 and the downstream W-3 gage (837 ha) over five sampling campaigns including a large (79 mm) fall storm, spring snowmelt, and three seasonally contrasting base flow periods. Filtered total Hg (THg), MeHg, and DOC concentrations increased in order base flow < snowmelt < fall storm, except that MeHg remained at baseflow levels during snowmelt. Ranges of median concentrations across sites for the five campaigns were THg, <0.2-4.1 ng L⁻¹; MeHg, $< 0.03-0.45 \text{ ng L}^{-1}$; and DOC, $0.8-14.0 \text{ mg L}^{-1}$. Humic-like DOM fluorescence components, as determined by parallel factor analysis (PARAFAC), dominated the fluorescence across sites and sampling campaigns. THg correlated strongly (r > 0.94) with these humic components, but even more strongly with bulk DOC and absorbance at 254 nm (UV₂₅₄; r > 0.96), and less strongly with protein-like DOM (0.7 < r < 0.9). MeHg correlated in the same order but less strongly with humic- (0.8 < r < 0.9) and protein-like (0.6 < r < 0.8) DOM. MeHg increased in summer, potentially in response to enhanced microbial production in warmer periods. MeHg formation may have been linked to protein-like DOM, but its transport was linked to humic-like DOM.

KEYWORDS

DOM quality, fluorescence, headwater stream, humic-like, methylmercury, PARAFAC, protein-like, total mercury

¹New England Water Science Center, U.S. Geological Survey, Montpelier, Vermont, USA

²Department of Earth Science, Dartmouth College, Hanover, New Hampshire, USA

³Department of Marine and Environmental Sciences, Northeastern University, Boston, Massachusetts, USA

⁴Department of Geology, University of Vermont, Burlington, Vermont, USA



1 | INTRODUCTION

Mercury (Hg) is a potent neurotoxin to humans and wildlife that bio-accumulates when converted to its organic and bioavailable form, methylmercury (MeHg; Eagles-Smith et al., 2018). Hg methylation in the aquatic environment and bioaccumulation in fish has long been recognized (Driscoll et al., 2007; Eagles-Smith et al., 2018; Fitzgerald & Clarkson, 1991). The terrestrial landscape and headwater streams deliver Hg to downgradient methylation hotspots (Chen et al., 2016; Krabbenhoft et al., 2005; Riscassi & Scanlon, 2011; Shanley et al., 2008). MeHg in forest headwater streams originates primarily from the surrounding catchment rather than from in-stream production (Branfireun et al., 2020; Bravo et al., 2017; Xu et al., 2019). Terrestrial methylation also introduces MeHg to the base of the terrestrial food web (Rimmer et al., 2019; Rodenhouse et al., 2019; Tsui et al., 2019).

Total mercury (THg) enters forest soils from atmospheric wet and dry deposition, but dry deposition typically dominates Hg accumulation in forest ecosystems (Risch et al., 2017; St. Louis et al., 2001). Dry Hg deposition enters the forest floor primarily as litterfall, from foliage that passively accumulates gaseous elemental Hg from the atmosphere throughout the growing season (Krabbenhoft et al., 2005; Navrátil et al., 2022; Rea et al., 2002). On reaching the soil, THg and MeHg are strongly held by soil organic matter (SOM; Navrátil et al., 2014; Obrist et al., 2011; Stoken et al., 2016), particularly by reduced sulphur (S) functional groups (thiols; Liem-Nguyen et al., 2017; Skyllberg et al., 2003). The strong Hg-SOM bond results in sequestering of Hg in organic soil such that only a small fraction of Hg deposition runs off in streamflow (Bishop et al., 2020; Krabbenhoft et al., 2005: Shanley et al., 2008). In a survey of 14 U.S. forest soils, Obrist et al. (2011) found that MeHg concentrations were highest in organic soil horizons, but that 88% of soil MeHg resided in the mineral soil (top 40 cm).

As in soils, THg and MeHg in waters are almost exclusively linked to organic matter (OM; Ravichandran, 2004), in particular humic aromatic OM of terrestrial origin containing reduced S groups (Liem-Nguyen et al., 2017; Skyllberg et al., 2003). The transport of THg and MeHg in subsurface and surface waters occurs in association with dissolved OM (DOM; Demers et al., 2010; Dittman et al., 2009, 2010; Krabbenhoft et al., 2005; Lavoie et al., 2019; Riscassi & Scanlon, 2011; Shanley & Bishop, 2012), largely in response to hydrologic forcing (Jiskra et al., 2017). Stream Hg export tends to be episodic as storms and transient high water tables flush DOM and Hg from organic soils (Bushey et al., 2008; Schelker et al., 2011; Shanley et al., 2002, 2008).

The importance of humic DOM to Hg mobility has been recognized for at least three decades. Mierle and Ingram (1991) linked Hg transport to humic substances through the positive correlation of Hg with water colour. Dittman et al. (2009) observed a strong correlation between THg and bulk dissolved organic carbon (DOC) among small streams over a range of flows, but they found an even stronger correlation between THg and the hydrophobic organic acid (HPOA) DOC fraction, which generally represents humic, aromatic DOM (Aiken

et al., 1992). Absorbance at 254 nm (UV $_{254}$) is another indicator of DOM aromaticity (Weishaar et al., 2003) and may be an even better predictor than bulk DOC or HPOA concentration (Dittman et al., 2009, 2010; Riscassi et al., 2011). Burns et al. (2013) found that THg was related strongly to UV $_{254}$ /DOC (specific UV absorbance or SUVA) in an Adirondack (New York) watershed, surprising because SUVA is a qualitative index of DOM quality. DOM fluorescence in the humic region (excitation 370 nm; emission 460 nm) was a strong predictor of Hg in an Alaskan glacial stream ($r^2 > 0.8$; Vermilyea et al., 2017). Finally, in a pan-European study of large rivers, THg had a strong association with soil-derived humic DOM (Bravo et al., 2018). Despite differing approaches, these diverse studies converge on the important role of humic OM in the movement of Hg on the landscape.

MeHg/THg is higher in soil solution and runoff than in soil, suggesting either that MeHg is more mobile than THg or that methylation occurs more readily in the aqueous phase (Skyllberg et al., 2003). MeHg export from soil to stream varies with seasonal MeHg supply due to greater production at higher temperatures (Hurley et al., 1995; Kronberg et al., 2016) and hydrologic connectivity to MeHg production hotspots (Branfireun & Roulet, 2002). In the European river study, Bravo et al. (2018) found that MeHg/THg was more related to microbially produced DOM than terrestrial DOM. Like THg, MeHg correlates with DOM, but variable MeHg supply weakens this relation (Jiskra et al., 2017; Lavoie et al., 2019) and MeHg may even dilute with flow (Bishop et al., 1995).

The methylation process has been well-studied in lake sediment (Bravo et al., 2017; Gilmour et al., 1992; Herrero Ortega et al., 2018; Watras et al., 1995) and to a lesser extent in stream sediment (Marvin-DiPasquale et al., 2009). Methylation occurs in soils similarly to sediments, the primary difference being variable water content in soils (Bigham et al., 2017). Methylation in forest soils is carried out by a diverse array of microbes, notably iron (Fe)- and sulphate (SO₄)-reducing bacteria (Gilmour et al., 2013; Tsui et al., 2019; Windham-Myers et al., 2014; Xu et al., 2019). Methylation is favoured by higher temperature (Ullrich et al., 2001) and higher soil moisture (Kronberg et al., 2016), and occurs under suboxic conditions (Bravo et al., 2017; Burns et al., 2014), including at microsites within otherwise oxygenated soils (Shanley et al., 2019). Vidon et al. (2014) found that variation in humic-like peak C, a fraction of fluorescent DOM, explained some of the variation in MeHg concentration.

DOM quantity and quality affect both MeHg formation and its subsequent mobility. Evidence is conflicting on whether OM facilitates or inhibits methylation (He et al., 2019), and Zhao et al. (2017) found that the effect may be opposing in different microbial strains. In Swedish lakes where sediment was primarily allochthonous, THg and MeHg in sediment correlated to terrestrially derived, humic DOM (Bravo et al., 2017). Methylation rates were low in these lake sediments, suggesting that the MeHg was terrestrially derived and was transported to the lake by allochthonous terrestrial DOM. In contrast, methylation rates were higher in lakes dominated by autochthonous sediment, where sediment Hg bound to algae-sourced DOM was more available for methylation (Bravo et al., 2017). In a coastal marine analog, Schartup et al. (2015) found that Hg methylation associated

with marine autochthonous DOM was greater than that associated with terrestrial DOM. Schartup et al. (2015) suggested that the larger molecular size of terrestrial DOM inhibited uptake of Hg into the cell where methylation occurs. Graham et al. (2013), in contrast, demonstrated in the laboratory that Hg bound to high-molecular weight aromatic DOM was more available for Hg methylation than other Hg-DOM complexes. Windham-Myers et al. (2014) showed that plant-derived labile OM stimulated methylation in rice paddies. Similarly, Levanoni et al. (2015) and Herrero Ortega et al. (2018) found that fresh OM sources stimulated methylation in beaver ponds.

Despite the long-held recognition that DOM quality is an important factor in Hg transport and Hg methylation, relatively few field studies have linked Hg measurements to detailed DOM characterization. Using fluorescence to characterize DOM quality, we investigated the response of Hg and MeHg in relation to DOM quality over a range of seasonal and hydrologic conditions (base flow, snowmelt, and a fall storm) at diverse locations within a forested headwater catchment. We isolated DOM into component fractions to identify the DOM component(s) most closely linked to THg and MeHg. Based on the known affinity of THg for terrestrial humic DOM and the known utilization of labile OM substrate by Hg-methylating microbes, we tested two hypotheses: (1) THg will correlate more closely to a specific humic-like DOM fluorescence component than to bulk DOC concentration; and (2) MeHg will correlate more closely to a protein-like DOM fluorescence component than to bulk DOC concentration. The long history of hydrologic and biogeochemical research at Sleepers River (Shanley et al., 2022), including past mercury studies, provided rich context for interpreting the dynamics of THg and MeHg and their interactions with DOM. This study is another application of the small watershed approach to investigate Hg cycling, as was done for the

five catchments of the USGS Water, Energy, and Biogeochemical Budgets (WEBB) programme (Shanley et al., 2008).

2 | METHODS

Sleepers River Research watershed (SRRW) in northeastern Vermont (Figure 1) has hosted hydrometeorological research since 1957, with a biogeochemical component since 1991 (Shanley et al., 2015; Shanley et al., 2022). SRRW has been a focus of previous Hg research (Dittman et al., 2009, 2010; Schuster et al., 2008; Shanley et al., 2002, 2008). Most of the sampling for the current study took place in the 41-ha W-9 catchment (Sebestyen et al., 2008; Shanley et al., 2004), which is 100% forested in northern hardwoods (Figure 1). The catchment is underlain by calcareous schist of the Waits River Formation, and is mantled by 1–4 m of dense, fine silty, locally derived glacial till (Shanley et al., 2004). W-9 ranges in elevation from 519 to 672 m, and it alternates steep hillslopes with relatively flat benches. This landscape variation gives rise to cryptic wetlands (Creed et al., 2003), including small swamps at stream heads, and pockets of deep organic soil horizons, including much of the riparian area.

The 4- to 6-week snowmelt period dominates the annual hydrograph at W-9, and flow recedes well into summer, punctuated by storms that can produce high peak flows at any time of year (Figure 2). The deep, poorly conductive glacial till helps to sustain base flow, so that the stream never ceases to flow in summer. The calcareous bedrock, which contains some pyrite, gives rise to a well-buffered calcium-bicarbonate-sulphate water, with Ca and acid neutralizing capacity (ANC) each exceeding 1000 μ eq L⁻¹ during low flow. The W-9 stream is flashy during storms, and DOC concentrations range

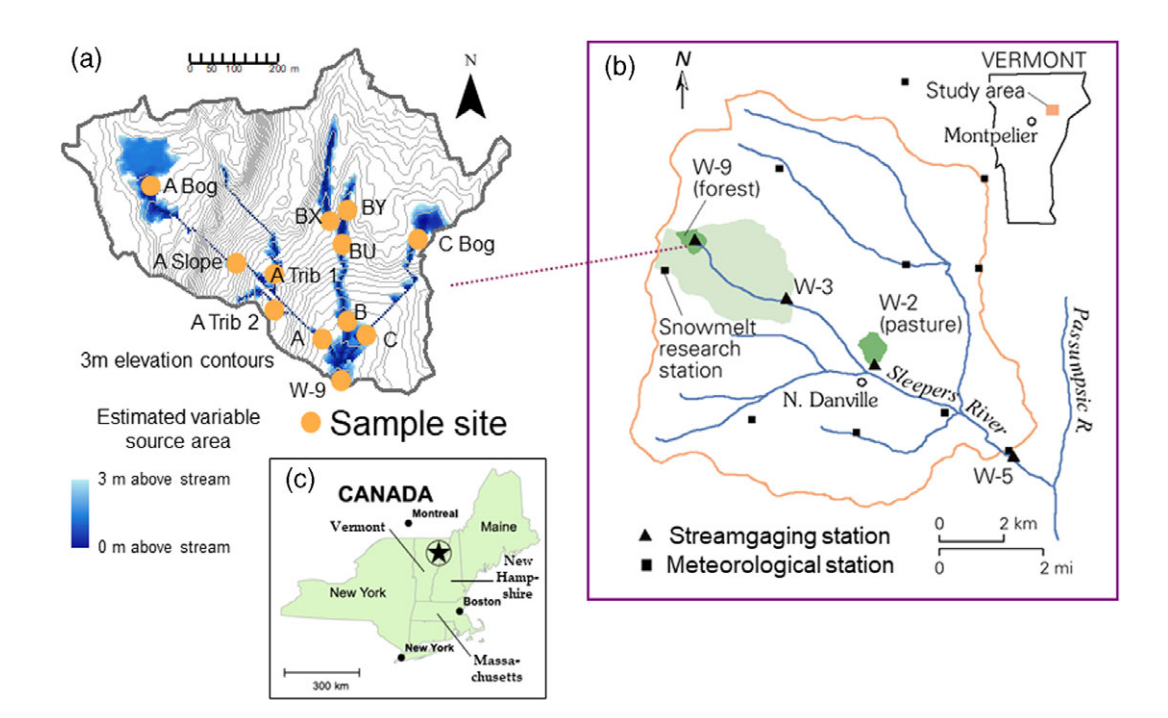


FIGURE 1 Map of (a) W-9 watershed, showing sampling sites, within (b) Sleepers River Research Watershed, and (c) locator map

.0991085, 2022, 5, Downloaded from https://onlinelibrary.wiley.com/doi/10.1002/hyp.14572 by University Of Vermont, Wiley Online Library on [19/06/2023]. See the Terms

and-conditions) on Wiley Online Library for rules of use; OA articles are governed by the applicable Creative Commons License

FIGURE 2 W-9 hydrograph for July 2017 through September 2018 showing the five sampling campaigns

TABLE 1 Physical conditions during the five sampling campaigns at Sleepers River Research Watershed, Vermont. Air and water temperatures are averages from the 30 days prior to sampling. Runoff is flow per unit area at W-9 at its sample time

Number	Campaign date	Time (EST)	Hydrologic condition	Runoff rate, $\mathrm{mm}\ \mathrm{h}^{-1}$	Air T, deg C	Water T, deg C
1	30 August 2017	12:40	Summer base flow	0.01	15.9	14.1
2	24 October 2017	21:50	Fall high flow	2.72	12.1	11.9
3	20 November 2017	11:40	Fall base flow	0.10	3.4	7.1
4	25 April 2018	18:50	Snowmelt	0.79	0.1	1.8
5	11 June 2018	11:00	Spring base flow	0.02	13.6	10.7

widely from near 1 mg L^{-1} at low flow to nearly 20 mg L^{-1} at the highest flows (Shanley et al., 2015).

To investigate the spatial and seasonal variability of Hg and DOM dynamics across this landscape, we conducted five synoptic sampling campaigns from August 2017 to June 2018. Each campaign sampled the same set of 11 small stream sites within W-9, as well as the W-9 gage site and the downstream gage at W-3 (Pope Brook; Figure 1), an 837-ha basin that includes ~20% agricultural land, primarily pasture for dairy farming. The W-9 sites included outlets to the headwater wetlands and most major and minor tributaries. The five dates included spring snowmelt (April), spring, summer, and fall base flow (June, August, and November), and a fall storm (October; Figure 2; Table 1). The fall storm was an exceptionally large event of 79 mm rainfall, occurring about 3 weeks after leaf fall on the evening of 24 October 2017. For this storm, we conducted the synoptic sampling high on the storm recession limb. In addition, we collected a time series of eight grab samples over the hydrograph at the W-9 gage.

Samples for Hg analysis were collected in square 1-L PETG bottles, thoroughly pre-rinsed with sample water, and kept chilled. The Hg samples were filtered (0.45- μ m GFF) and acidified to 0.4% hydrochloric acid (HCl), then analysed for Hg within 24 h at Dartmouth College. For MeHg analysis, ~30 ml of sample was weighed into an acid-washed brown glass septa vial. A 0.2-ml aliquot of citrate buffer was added to each vial, the sample was buffered to pH 4.5 with potassium hydroxide (KOH), and 30 μ l of ethylating reagent was added. Waters were analysed for MeHg by a Tekran 2700 automated MeHg analyser. The mean \pm standard error (SE) relative percent difference (RPD) for duplicate samples was 9 \pm 2% (n = 11). Mean aqueous MeHg spike and standard recoveries were 89 \pm 3% (n = 11) and 93 \pm 1% (n = 4). The limit of detection for MeHg was 0.006 ng L $^{-1}$.

THg was analysed using a modification of EPA method 1631 (U.S. EPA, 1999). Samples (~25 ml) were weighed into clear septa vials and digested chemically with bromine monochloride (BrCI) and subsequently neutralized with hydroxylamine hydrochloride (NH2OH·HCl). Sample Hg was reduced to Hg⁰ with stannous chloride (SnCl₂), and samples were analysed by a MERX-T automated total mercury analyser, with cold vapour atomic fluorescence detection (Brooks Rand Instruments). Sample results were corrected for field and preparation blanks as appropriate. The mean ± SE RPD for duplicate samples was $9 \pm 3\%$ (n = 6). Mean aqueous THg spike and standard recoveries were $104 \pm 6\%$ (n = 6) and $109 \pm 2\%$ (n = 14). The limit of detection for THg was 0.2 ng L^{-1} . To investigate variations in water sources across discharge conditions, we analysed major elements: aluminium (AI), calcium (Ca), iron (Fe), potassium (K), magnesium (Mg,) manganese (Mn), sodium (Na), phosphorus (P), sulphur (S), and strontium (Sr), by inductively coupled plasma optical emission spectroscopy (Thermo Iris Intrepid 2) in 7-ml subsamples acidified to 5% nitric acid (HNO₃).

For DOM, all sample materials were pre-cleaned with acidified water, triple rinsed with pure deionized water, and rinsed with sample water prior to collection. Grab samples for DOM were syringe-filtered (0.22- μ m, Polyethersulphone, Waterra) immediately on site into 60-ml glass amber bottles. Separate aliquots were collected through the same filter in 125-ml PE bottles for major solutes. Aliquots of each sample for analysis of DOC concentration were transferred to pre-combusted glass vials and acidified to pH 2 with 6N HCl and refrigerated (6°C) in the dark until analysis within 4 weeks of sampling. DOC was measured as nonpurgeable organic carbon using a high-temperature catalytic combustion procedure (Shimadzu Total Organic Carbon Analyser, Columbia, MD, USA). A 1000 mg L $^{-1}$ stock DOC solution for calibration standards was prepared using potassium hydrogen phthalate and potassium nitrate.

Absorbance and fluorescence of DOM were measured on filtered, non-acidified sample aliquots using an Aqualog™ Fluorescence and Absorbance Spectrometer and 1-cm quartz cuvettes (Horiba, Irvine, CA, USA). Samples were stored at 6°C in the dark and equilibrated to room temperature (21–23°C) prior to analysis within 2 weeks of sampling. Chromophoric DOM (CDOM) absorbance spectra were measured from 200 to 600 nm and blank-corrected using ultrapure water (Milli-Q, Millipore). Decadic and Naperian absorption coefficients were calculated according to Hu et al. (2002). Specific UV absorbance at 254 nm (SUVA₂₅₄, L mg C⁻¹ m⁻¹), was calculated by dividing the decadic absorption coefficient at 254 nm (m⁻¹) by the DOC concentration (mg L⁻¹) for each sample (Weishaar et al., 2003). Spectral slopes of absorbance spectra and slope ratios were calculated according to Helms et al. (2008) (Table S1).

Three-dimensional fluorescence spectra ranged from 242 to 596 nm excitation and 212 to 619 nm emission. Excitation-emission matrices (EEMs) were corrected for instrument-specific effects and solution interference (inner filter effect) using the Aqualog software correction functions and according to Murphy et al. (2013). As raw absorbance values never exceeded 0.4 absorbance units, no samples required dilution (Kothawala et al., 2013). EEMs were blank subtracted using fluorescence spectra of ultrapure Milli-Q water (Millipore) collected daily. Lamp and cuvette performance were assessed daily and each pre-processed EEM was normalized to Raman peak area (Lawaetz & Stedmon, 2009). Rayleigh and Raman scatter interferences were removed prior to replacement using spline interpolation (StaRdom package in R, version 1.1.1; Pucher et al., 2019).

Parallel factor analysis (PARAFAC) was conducted on 72 preprocessed EEMs to characterize fluorescent DOM (FDOM) quality using StaRdom (Pucher et al., 2019). PARAFAC models are useful for identifying uncorrelated fluorophore components contributing to the overall DOM fluorescence within a group of samples (Bro, 1997). All EEMs were cut to ranges of 250-550 nm for excitation and 250-600 nm for emission, and data were restricted to non-negative values to reduce instrument noise associated with low-fluorescing samples during model development. Each EEM was normalized to its total fluorescence signal to reduce the influence of DOM concentration during model development. Conventional fluorescence peaks (B, T, A, M, C) were also extracted from corrected EEMs using StaRdom package functions according to the references therein (Coble, 1996; Ohno, 2002). In addition to the absorbance indices mentioned earlier, we calculated the fluorescence index, FI (McKnight et al., 2001), humification index, HIX (Huguet et al., 2009), and freshness index (Zsolnay et al., 1999) (see Table S1 for details).

Principle component analysis (PCA) was used as a visualization tool to identify relations between the large number of chemical variables, and groupings of individual samples. DOM metrics (DOC, UV_{254} , fluorescence components), major element concentrations, and Hg and MeHg were included in the PCA. The qualitative optical indices (e.g., SUVA, FI) were not used to drive the PCA but were laid on as ancillary variables. All data were log transformed to meet assumptions of normality and scaled prior to performing the PCA using the FactoMineR package in R.3.5.3.

A six-component PARAFAC model (Figure S1) best described the dataset and was validated using three combinations of random samples in a split-half analysis. Tucker's congruency coefficients among all components averaged 0.96 with a standard deviation of 0.07. Since no further investigation of the chemical composition of fluorescent DOM was performed for this study, PARAFAC model components were classified according to known fluorescence peaks (Fellman et al., 2010; Hansen et al., 2016). Our PARAFAC model matched 36 previously published models in the Openfluor online database (minimum similarity score: 0.97; Murphy et al., 2014). Of the six components, four (C1, C2, C3, and C4) represented humic-like DOM. C2 corresponded closely to the classic Peak M while C1 and C3 corresponded closely to the classic Peak A (Coble, 1996). C4 was a blueshifted humic-like peak. C5 and C6 were protein-like or fresh-like components; C6 corresponded to the classic Peak T. We term these components 'protein-like' based on classic literature descriptions of similar components (e.g., Fellman et al., 2010). These components are usually associated with either biolabile or autochthonous OM, but may also include a suite of other DOM molecules (Stubbins et al., 2014), and are not necessarily proteins or microbially

3 | RESULTS

derived OM.

3.1 | THg and MeHg spatial concentration patterns

Filtered total Hg ranged from 0.01 to 7.9 ng L $^{-1}$ across all sites and campaigns (Figure 3b). Median THg across the 13 sites ranged from 0.04 to 1.23 ng L $^{-1}$, with the highest THg at the outlet of A Bog (a \sim 1-ha swamp), the largest wetland area in the catchment. Within each site, THg ranged over more than one and in some cases nearly two orders of magnitude, and was positively aligned with flow during the five sampling campaigns. The five sites in the steeper subcatchment A generally had higher THg than other sites, but differences were not significant (p > 0.05).

Filtered MeHg was quite low, ranging from <0.006 to 0.14 ng L $^{-1}$ (Figure 3c). Site median MeHg ranged from 0.008 to 0.05 ng L $^{-1}$. Within-site variation of MeHg was less than that of THg, generally close to or within one order of magnitude. Median MeHg values across sites were also less variable, within a factor of two or three, except for the wetland outlet, A Bog, which was several-fold higher. A Bog and C Bog, the other swamp outlet, maintained consistently high MeHg concentrations during all sampling campaigns.

The MeHg/THg ratio, sometimes termed the methylation efficiency (Krabbenhoft et al., 1999), ranged from 0.5% to 70% (Figure 3d). Consistent with the lower spatial variability in MeHg, the pattern of MeHg/THg was inverse to that of THg, with lower values in sub-catchment A and higher values in sub-catchment B. The range within each site was generally an order of magnitude, but up to two orders at a few sites. Site median MeHg/THg ranged from 1.6% to 11.9%. With a few exceptions, MeHg/THg converged on a lower limit near 1% (Figure 3).

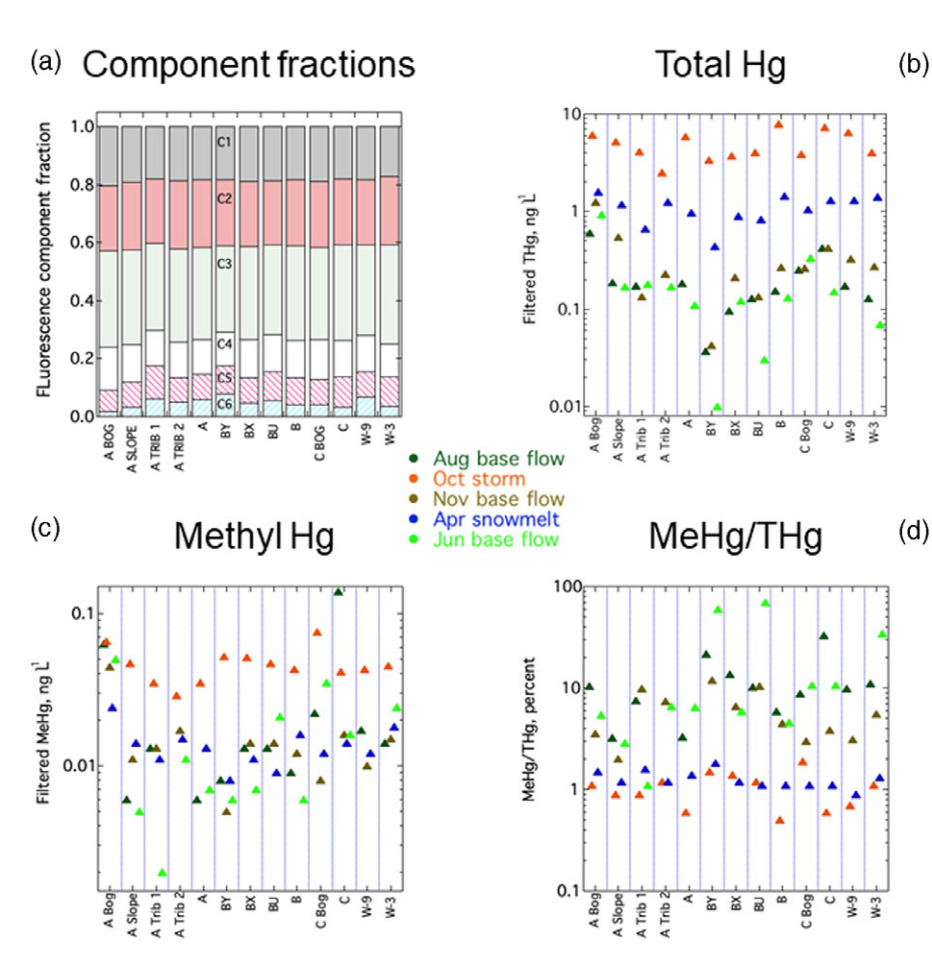


FIGURE 3 (a) Spatial distribution of average relative PARAFAC component fractions; and (b) THg, (c) MeHg, and (d) MeHg/THg across sampling sites. Except for a few missing samples, n=5 for each site, that is, one sample from each of the five sampling campaigns. Within each site, values are in chronological order along the x-axis

3.2 | THg and MeHg temporal concentration patterns

THg concentration during the large October 2017 storm exceeded 2 ng L^{-1} at all sites (Figure 4b), which was severalfold greater than during the April 2018 snowmelt, the other high-flow period sampled. THg was generally more than an order of magnitude lower and uniformly less than 1 ng L^{-1} during the three base-flow periods, and was lower in the late spring baseflow (June 2018) than the late summer and late fall periods in 2017. There was strong consistency in the relative magnitude of THg across sites among the campaigns (Figure 4b; little 'crossing' of lines).

The highest MeHg concentration at each site generally occurred during the large October storm, when MeHg concentrations at all sites exceeded 0.028 ng L $^{-1}$ (Figure 4c). However, MeHg increased only twofold to fourfold during the fall storm relative to the other campaigns, compared to the order-of-magnitude or more increase in THg. With the exception of a few outliers, MeHg concentration ranged over less than an order of magnitude and centered near 0.01 ng L $^{-1}$ for the other four dates. Unlike THg, MeHg was not elevated during the April 2018 snowmelt. MeHg at A Bog was significantly greater (*t*-test, *p* < 0.005) than at other sites (Figure 4c). C bog, the other wetland outlet, had the next-highest median MeHg.

The MeHg/THg ratio was markedly higher during the three base flow periods than the two high-flow events (Figure 4d). MeHg/THg

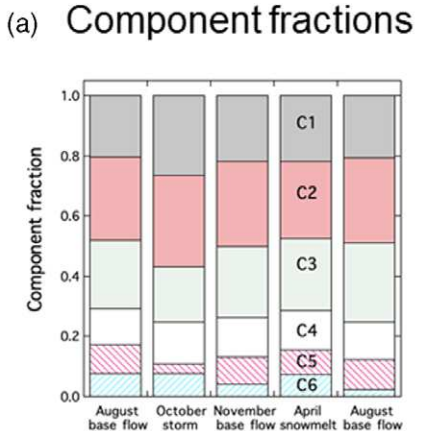
was more variable at base flow, spanning an order of magnitude in percentage, and was always at least 10% at some sites. It was generally lower and only marginally exceeded 10% during the coldest base flow period in November 2017. MeHg and THg were both elevated at high flow, but MeHg/THg decreased to \sim 1%, and at some sites was <1% during the large fall storm. MeHg/THg correlated positively to the 30-day prior average water temperature (p < 0.01 with two outliers removed) and inversely with flow (both variables log-transformed; p << 0.001).

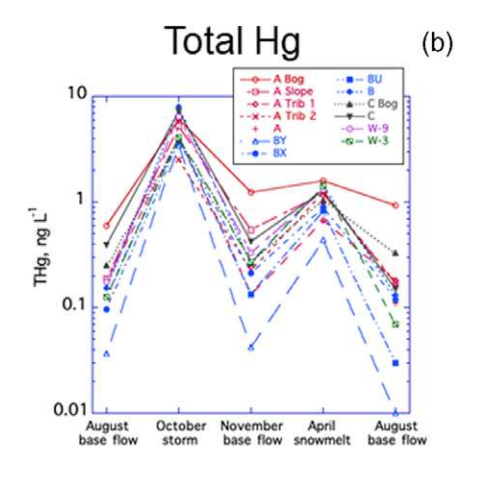
At the W-9 stream gage over the large fall storm hydrograph, THg increased rapidly from 0.4 ng L $^{-1}$ at pre-storm base flow to a maximum of 6.7 ng L $^{-1}$ just after peak flow (Figure 5). THg remained elevated at 2.5 ng L $^{-1}$ 9 hours after the hydrograph peak, when flow had receded from nearly 4 to 0.2 mm hr $^{-1}$. MeHg behaved non-systematically, increasing from 0.06 ng L $^{-1}$ pre-storm to 0.09 ng L $^{-1}$ as flow began to rise, then decreasing to 0.04 ng L $^{-1}$ at peak flow and remaining near that value throughout the recession (Figure S2).

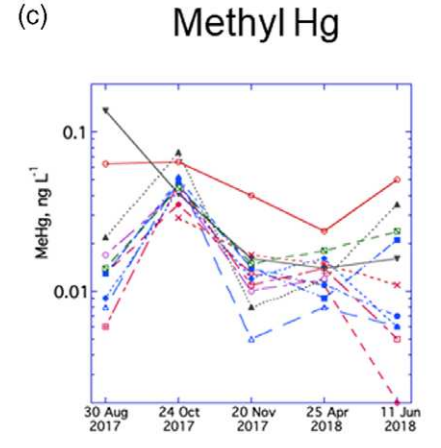
3.3 | DOC and DOM optical quality dynamics

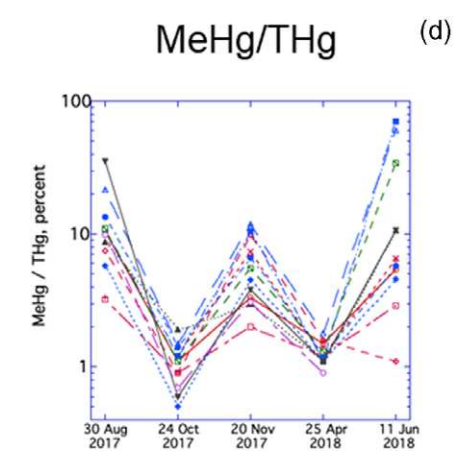
Across all samples, decadic UV_{254} absorbance coefficient varied from 1.6 to 90 m^{-1} . Minimum fluorescence intensity across PARAFAC components varied from 0.00 to 0.36, while maximum intensities varied from 0.30 to 1.85, in Raman-normalized fluorescence units (R.U.).

FIGURE 4 (a) Temporal distribution of average relative PARAFAC component fractions; and (b) THg, (c) MeHg, and (d) MeHg/ THg across the five sampling dates. Except for a few missing samples, n=13 with one sample from each site and date. The x-axis on panels (a) and (b) denote the month and hydrologic condition, while panels (c) and (d) show the corresponding sampling dates. Sampling locations are shown in Figure 1









Analogously, minimum fluorescence intensity for the Coble peaks A (0.07 R.U.), C (0.04 R.U.), and T (0.0003 R.U.) were approximately two orders of magnitude lower than their respective maximum intensities of 3.2, 2.1, and 0.4 R.U. These ranges match or exceed those in other temperate forested natural waters (Fellman et al., 2010; Yamashita et al., 2011, and references therein). DOC exhibited a similar dynamic range as THg, ranging overall from 0.4 to 22.4 mg L⁻¹ (site medians 0.8 to 14.0 mg L^{-1}), and had a similar strong positive correlation with flow. DOM quality was dominated by the humic-like components (C1-C4) across sites (Figure 3a) and across campaigns (Figure 4a). C1, C2, and C3 were present in roughly equal amounts and collectively made up 70%-80% of total fluorescence intensity at most sites and dates (average 73% ± 3%). C3 varied inversely to C1 and C2 to maintain this relatively constant fraction. C4, the blue-shifted humic component, ranged tightly from 10% to 15%. C5 and C6, the protein-like components, were the most variable, each varying independently from near 0 to \sim 15% (Figure S3). Spectral slope ($S_{275-295}$) over the study ranged from 0.011 to 0.018. The highest $S_{275-295}$ values (>0.013; Figure S4) generally occurred at base flow. The lower $S_{275-295}$ values at higher flows were associated with increases in C1-C4 and decreases in C5-C6 (Figure S5).

DOC during the October high-flow campaign was generally an order of magnitude higher, and both the humic and protein-like DOM fluorescence component proportions shifted in composition relative

to the other campaigns (Figure 4a). Among the humic fractions, percent C1 and C2 increased and C3 decreased, but C1 + C2 + C3 remained similar to the other campaigns. Among the protein-like fractions, percent C6 was higher during the fall storm than the other 4 dates, while C5 decreased from its typical value of $\sim 10\%$ to near 3%. Over the storm hydrograph at W-9, the protein-like C6 component spiked from 7% to 22% on the rising limb before falling gradually and progressively back to 6% (Figure 5b). The humic-like C1 and C2 components remained at a fairly constant percentage, while percentages of C3, C4, and C5 collectively increased or decreased to compensate for the variation in C6 (Figure 5b).

3.4 | THg and MeHg behaviour relative to other solutes and DOM quality

THg, DOC, DOM components, and flow were all strongly intercorrelated. (Note: all r values reported in this section are Pearson's r for linear regression, and all p values are <0.001 unless otherwise indicated [Table 2].) Over all sites and dates, THg had its strongest correlations with DOC and UV₂₅₄ (r=0.957 in both cases; Figure 6). Among DOM fluorescence components, THg correlated most strongly with intensities of C1 (r=0.940) and C2 (r=0.937), and lowest with intensities of the protein-like components C5 (r=0.708) and C6

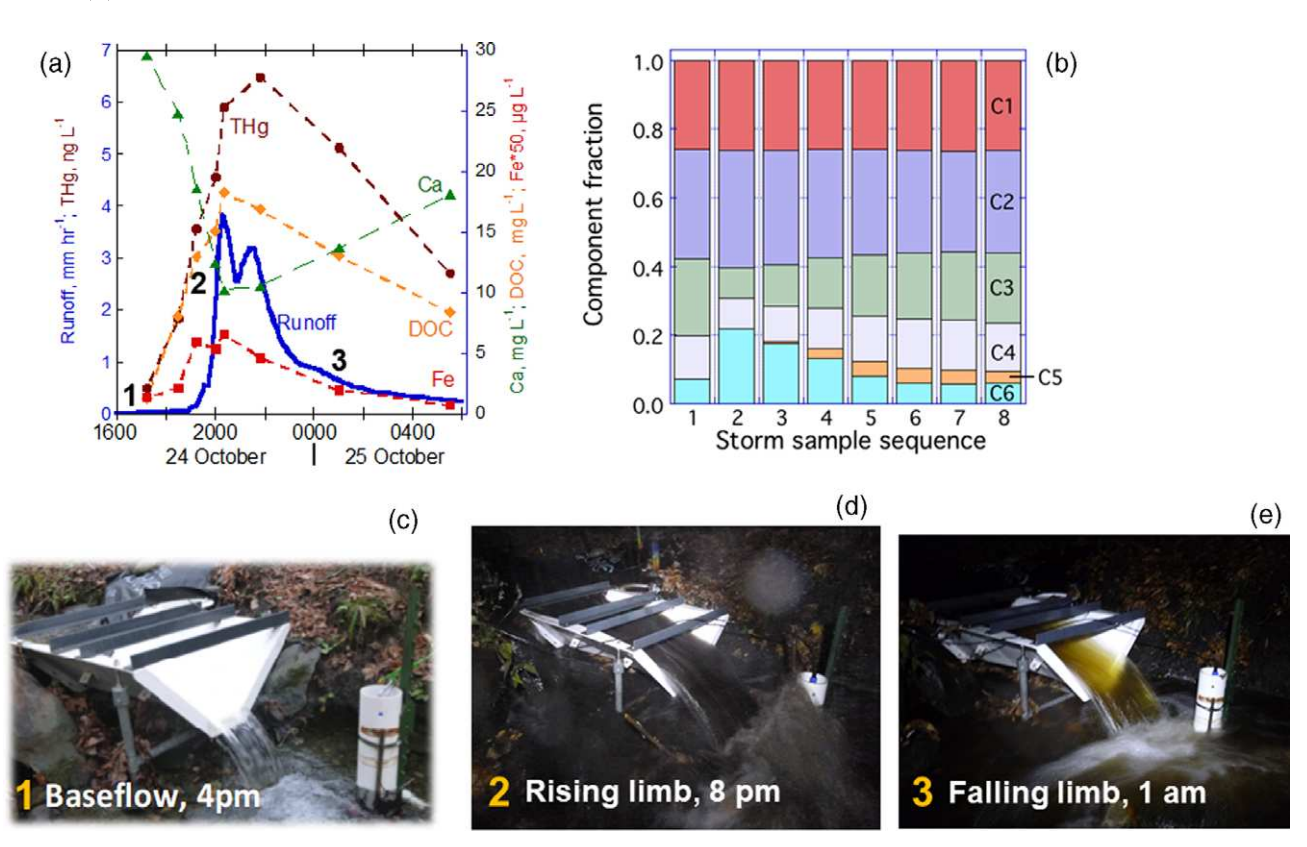


FIGURE 5 Large 79-mm rainstorm of 24–25 October 2017, showing (a) W-9 stream hydrograph and time series of THg, dissolved organic carbon, Ca, and Fe concentrations, and (b) PARAFAC component fractions. The bold numbers on the hydrograph in panel A correspond to the photos in panels (c), (d), and (e). The photos show the flume on 13-ha tributary B of the 41-ha W-9. Note the clear base flow (c), high-sediment rising limb (d), and low sediment, high colour falling limb (e). Photographs by Kevin A. Ryan

(r = 0.874; Figure 6; Table 2). THg did not correlate more strongly with any additive combinations of components than with C1 or C2 individually. THg correlated nearly as strongly with the intensities of the conventional humic-like peaks A, C, and M (0.923 < r < 0.937). The largest outliers in all relations were the wetland swamp outlets A Bog and C Bog, which had less Hg for any given DOM metric (Figure 6). Variation in THg concentrations across sites was large relative to variation in DOM composition (Figure 3a).

MeHg correlated with DOC, UV $_{254}$, and all fluorescence-based DOM components somewhat less strongly than THg. If one high-MeHg outlier is removed, all correlation r values increase by >0.2 to 0.87–0.88 for the humic-like C1-C4, 0.80 for the protein-like C5, and 0.72 for the protein-like C6 (Figure 7; Table 2). Unlike THg, MeHg correlated less strongly with DOC (r=0.846) and UV $_{254}$ (r=0.843) than with the fluorescent humic components (Figure 7).

THg and MeHg correlated inversely and less strongly with the DOM quality indices FI, $S_{275-295}$, and freshness index (Table 2). MeHg had a significant inverse correlation with freshness index (r=-0.49), and an even stronger one for the storm time series (r=-0.89; Figure 8). Freshness index is an indicator of fresh autochthonous DOM (Huguet et al., 2009). THg had a significant inverse relation with FI (r=-0.50), and again a stronger one for the storm time series (r=-0.94; Figure S6). THg had an inverse relation with $S_{275-295}$ and a positive but non-significant relation with HIX

(Figure S4). MeHg had a significant positive relation with HIX (Table 2). See Supporting Information for further discussion of THg and MeHg in relation to the DOM quality indices.

During the October storm hydrograph at W-9, THg closely tracked DOC (and Fe) concentration, but varied inversely with Ca, which diluted with increasing flow (Figure 5). Compared to the overall relations across the campaigns, THg over the storm hydrograph correlated slightly lower with DOC (r=0.95), but even more strongly with UV₂₅₄ (r=0.99) and the humic fractions C1-C4 (0.91 < r < 0.99). THg did not correlate with the protein-like C6, which peaked well in advance of the THg peak during the storm (Figure S2). MeHg behaviour was decoupled from THg and DOM over the storm hydrograph. While THg maintained strong positive correlations with DOM components for the eight storm samples, the MeHg-humic linkage present in the synoptic sampling broke down over the storm hydrograph. MeHg in general correlated negatively with the humic component intensities (Table 2) during the storm, and after an initial flushing, MeHg tracked the diluting base cations (Figure S2).

In the PCA, PC1 explained 60.2% of the variance and PC2 explained 16.8% of the variance (Figure 9). MeHg and THg bracket DOC, $\rm UV_{254}$, and all the DOM fluorescence components and conventional EEM peaks with strong positive PC1 loadings, while the autochthonous indices FI, SR, and freshness, had strongly negative PC1 loadings and grouped with sulphur. PC2 had positive loadings

TABLE 2 Pearson's r correlation coefficients and corresponding p values for regressions of filtered THg and MeHg on all DOM-related metrics measured in this study

	THg				MeHg					
	Synoptic surveys		October hydrograph		Synoptic surveys		October hydrograph		Synoptic - outlier removed	
	r	р	r	р	r	р	r	р	r	р
DOC	0.957	<0.0001	0.953	0.0003	0.600	<0.0001	-0.253	0.546	0.846	<0.0001
UV ₂₅₄	0.957	<0.0001	0.988	<0.0001	0.592	<0.0001	-0.401	0.325	0.843	<0.0001
C1	0.940	<0.0001	0.986	<0.0001	0.620	<0.0001	-0.402	0.323	0.877	<0.0001
C2	0.937	<0.0001	0.967	<0.0001	0.630	<0.0001	-0.319	0.441	0.885	<0.0001
C3	0.890	<0.0001	0.955	0.0002	0.631	<0.0001	-0.659	0.075	0.883	<0.0001
C4	0.930	<0.0001	0.981	<0.0001	0.620	<0.0001	-0.577	0.134	0.875	<0.0001
C5	0.708	<0.0001	0.917	0.0014	0.584	<0.0001	-0.622	0.074	0.795	<0.0001
C6	0.874	<0.0001	0.371	0.37	0.485	<0.0001	0.511	0.196	0.717	<0.0001
Peak B	0.763	<0.0001	0.020	0.96	0.350	0.0045	0.728	0.041	0.648	0.0045
Peak T	0.912	<0.0001	0.672	0.068	0.438	0.0003	0.232	0.580	0.801	0.0003
Peak A	0.923	<0.0001	0.990	<0.0001	0.497	<0.0001	0.481	0.227	0.882	<0.0001
Peak M	0.937	<0.0001	0.961	0.0002	0.498	<0.0001	-0.291	0.484	0.879	<0.0001
Peak C	0.931	<0.0001	0.989	<0.0001	0.494	<0.0001	-0.473	0.236	0.877	<0.0001
FI	-0.506	<0.0001	-0.938	0.0006	-0.340	0.007	0.648	0.082	-0.508	<0.0001
S ₂₇₅₋₂₉₅	-0.543	<0.0001	0.492	0.216	-0.235	0.0655	-0.301	0.468	-0.476	0.0001
SR	-0.731	<0.0001	-0.617	0.103	-0.528	<0.0001	0.912	0.0016	-0.736	<0.0001
Freshness index	-0.786	<0.0001	0.085	0.84	-0.491	<0.0001	-0.867	0.0053	-0.731	<0.0001
HIX	0.320	0.011	0.318	0.443	0.428	0.0005	-0.899	0.0024	0.520	<0.0001
SUVA	-0.077	0.55	-0.116	0.78	-0.229	0.074	-0.588	0.0125	0.126	0.333

Note: October hydrograph refers to the eight samples collected at the W-9 gage during the large October 2017 storm. MeHg regressions performed with and without one high outlier. DOC is dissolved organic carbon; FI is florescence index; $S_{275-295}$ is spectral slope; SR is spectral slope ratio; HIX is humification index; SUVA is specific UV absorbance (UV₂₅₄/DOC).

Abbreviations: DOC, dissolved organic carbon; DOM, dissolved organic matter.

for a cluster of base cations (Na, Ca, Sr, Mg) and another cluster of soil-derived and/or redox-and pH-sensitive elements (Fe, Mn and Al) and nutrients (nitrogen [N] and P), as well as HIX. THg plotted directly opposite the base cation group and tightly between the DOM-related cluster and discharge along PC1. MeHg plotted on the other side of the DOM cluster from THg, proximal to the soil-derived solutes Fe and Mn.

Samples were widely distributed along both axes among the variables in PC space, but they grouped strongly by campaign date rather than by site, suggesting greater temporal than spatial cohesiveness in the dynamics and controls on THg and MeHg movement. Summer, fall and spring base flow samples loaded negatively along the primary axis associated with low discharge. The elevated MeHg, THg, and Fe at the wetland outlets caused each cluster to spread into positive PC1 space. The October storm and snowmelt samples loaded positively on the high-discharge primary axis. Samples from the two coldest temperature campaigns, fall baseflow and snowmelt, loaded negatively along the second axis, separated from the spring, summer and fall storm samples. These samples had low MeHg, even during the high snowmelt discharge in the spring.

4 | DISCUSSION

In this study, we characterized DOM in detail to assess whether specific DOM components governed THg and MeHg cycling in a forested catchment. At the Sleepers River W-9 catchment, THg varies dynamically in strong association with DOM and correlates strongly with the HPOA fraction of DOM, whereas MeHg varied more independently of DOM (Shanley et al., 2008). Here, we conducted Hg sampling jointly with DOM fluorescence characterization to test whether THg and MeHg associate preferentially with specific DOM fluorescence components, and whether these components differ for THg and MeHg.

4.1 | Overall relations and PCA interpretation

Variable clusters in the PCA (Figure 9) aligned by discharge along the strongly dominant PC1 and by temperature along PC2. The grouping of THg with DOM components and soil-related (Fe, Al, TDN, K, HIX) clusters with positive PC1 loadings, coupled with negative PC1 loadings for the base cation cluster, suggested flushing of THg and DOM from shallow soils and dilution of groundwater under high-flow

0991085, 2022, 5, Downloaded from https://online.library.wiley.com/doi/10.1002/hyp.14572 by University Of Vermont, Wiley Online Library on [19/06/2023]. See the Term

on Wiley Online Library for rules of use; OA articles are governed by the applicable Creative Commons License

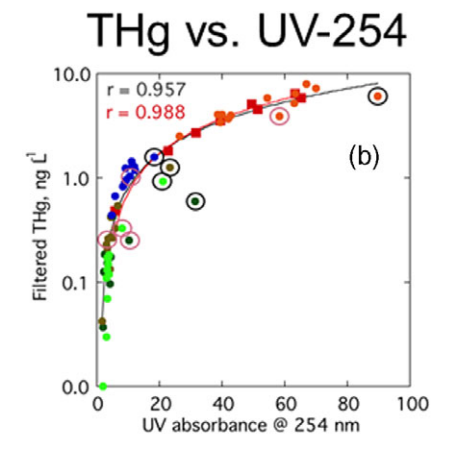
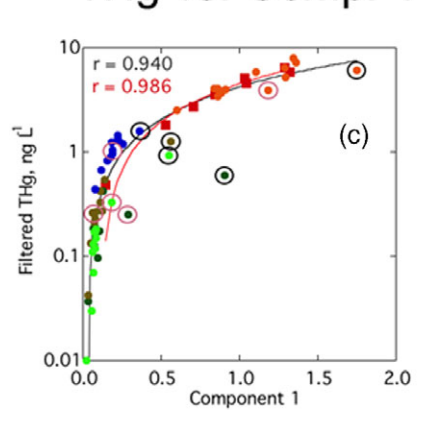
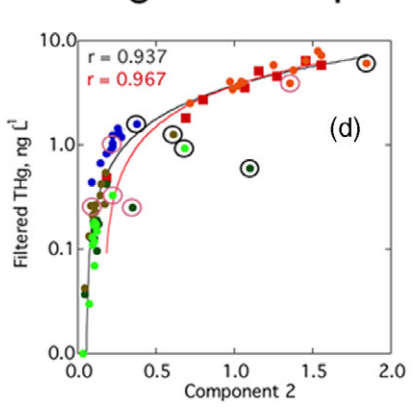


FIGURE 6 THg versus (a) dissolved organic carbon, (b) UV_{254} (m $^{-1}$), (c) PARAFAC component 1 (R.U.), and (d) PARAFAC component 2 (R.U.), for samples over the five campaigns, and for the 24–25 October time series at W-9 weir (data points, regression line, and r-value all in red for time series). Regression lines shown are linear in arithmetic space. Circled points represent outlets to headwater swamps

THq vs. Comp. 1



THg vs. Comp. 2



conditions. MeHg loaded positively on flow and also on temperature, and it aligned (inversely) with the authochthonous variable cluster, suggesting MeHg is also flushed from soils in association with terrigenous DOM, but that its supply is limited in cooler temperatures. MeHg associated more closely than THg with Fe and Mn, supporting that it is sourced from reducing soils (Figure 9). The clustering of streamwater samples by campaign date in the PCA supported the discharge and seasonal temperature controls.

4.2 | Why does bulk DOC outperform humic OM in predicting THg?

Hypothesis 1 posited that THg would associate more strongly with one or more of the humic-like DOM fluorescence components than to bulk DOC or UV_{254} . Filtered THg concentration indeed correlated strongly to the four humic-like components identified by the PARA-FAC analysis, and more weakly to the two protein-like components. However, except during the October storm time series (Figure 6), THg correlated more strongly with DOC and UV_{254} than with any of the PARAFAC components (Figure 3) or the conventional humic EEM peaks A, C, and M. Thus, hypothesis 1 was refuted.

The failure of a specific humic component to emerge from bulk DOC as the 'best' predictor of THg may follow from the strong

similarity of DOM source environments in this small headwater catchment. DOC and UV $_{254}$ analyses are more robust than the data-rich but less reliable/more nuanced fluorescence-derived components (Stubbins et al., 2014), which likely overlap in this relatively homogenous headwater landscape. Fourier transform ion cyclotron resonance-mass spectrometry (FTIRC-MS) is a tool that can identify specific organic molecules transporting Hg (Chen et al., 2017). Underscoring OM diversity, FTIRC-MS has revealed opposing hysteresis loops during storms for specific molecules in this catchment (Wagner et al., 2019). The strong THg-UV $_{254}$ correlation was consistent with earlier findings of Dittman et al. (2009) in this catchment, that THg correlated more strongly to UV $_{254}$ than to other measures of DOM, including hydrophobic acid. Lescord et al. (2018) demonstrated convincingly that THg associates with different DOM components in different settings in a large heterogeneous basin in Canada.

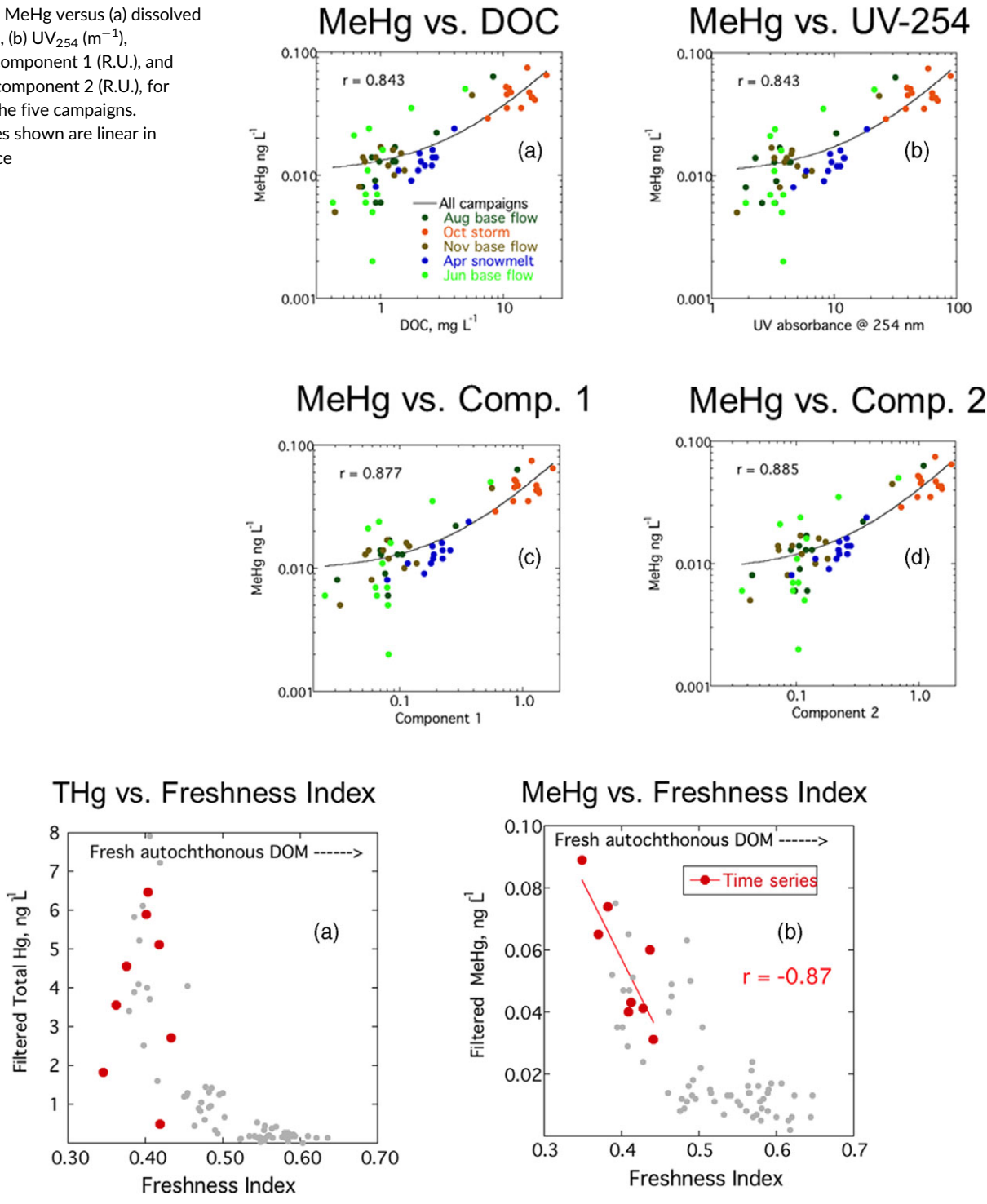
4.3 | Hg-OM in soil versus solution

The strong relation of THg to humic substances is well-established (Lavoie et al., 2019; Ravichandran, 2004) and is so prevalent in the environment (Demers et al., 2013; Dittman et al., 2009) that Hg movement is universally associated with humic OM movement. The affinity of Hg for reduced S groups (i.e., thiols) in OM far exceeds that

0991085, 2022, 5, Downloaded from https://online.library.wiley.com/doi/10.1002/hyp.14572 by University Of Vermont, Wiley Online Library on [19/06/2023]. See the Term

of use; OA articles are governed by the applicable Creative Commons License

FIGURE 7 organic carbon, (b) UV_{254} (m⁻¹), (c) PARAFAC component 1 (R.U.), and (d) PARAFAC component 2 (R.U.), for samples over the five campaigns. Regression lines shown are linear in arithmetic space



(a) THg, and (b) MeHg versus freshness index, with October storm time series plotted in red. Note the significant regression and r value for MeHg

of all other ligands and inorganic anions (Liem-Nguyen et al., 2017; Ravichandran, 2004; Skyllberg et al., 2003), and the population of reduced S binding sites far exceeds the supply of Hg (Skyllberg et al., 2003). Thiol groups tend to occur in a wide array of humic compounds (Haitzer et al., 2003), which may preclude the emergence of a single dominant humic component that associates with Hg.

Hg desorption is a slow process (Jiskra et al., 2014), so the Hgthiol bond in soil OM (Hg-RSH) is likely to be preserved in the aqueous phase upon solubilization, rather than Hg desorbing and forming a new DOM complex. While Chiasson-Gould et al. (2014) observed frequent ligand exchange with 'new' Hg, the stable OM-Hg complexes in forest soils should remain intact and move as a stable complex on

FIGURE 9 Principal component analysis (PCA) with like variables grouped by colour shading (left panel) and samples (right panel) differentiated by the five sampling campaigns. Samples from A bog (A) and C bog (C) for each campaign are indicated. Qualitative indices (HIF, FI, S₂₇₅₋₂₉₅, SR, and freshness; see text and Table 2 and Table S1 for definitions) were not used to drive the PCA, but were overlain as ancillary variables

dissolution. If ligand exchange occurred and a new Hg-RSH bond were to form, it would cause enrichment of heavy Hg isotopes in the dissolved phase. No such isotopic fractionation occurred at boreal sites in northern Sweden (Jiskra et al., 2017). Instead, the Hg isotopic evidence, the OM radiocarbon signal (indicating post-bomb C), and the Hg/C ratio collectively indicated that stream Hg and its associated OM were jointly sourced from the soil Oe horizon (Jiskra et al., 2017). In sum, Hg and DOM are released from a common source in soil OM, and the specific Hg-humic association present in the soil persists as a complex in solution. The organic ligand maintains the Hg in solution, preventing Hg from immobilization by soil OM. Hg/C ratios generally increase with depth in the soil (Navrátil et al., 2014; Obrist et al., 2009), indicating that Hg persists as OM is mineralized, owing to its strong preference for solid phase OM (log K_d for soils 3.5–4.8 for THg and 1.3–3.8 for MeHg; Lyon et al., 1997).

4.4 | Contrasting MeHg and THg dynamics

MeHg concentrations closely tracked THg concentrations and also correlated, albeit less strongly, with humic DOM components. The poorer alignment of MeHg to DOM is a common finding (Brigham et al., 2009; Schwesig & Matzner, 2001; Shanley et al., 2008), and was likely related to the seasonal production cycle of MeHg. Due to its microbial origin, MeHg was more linked to the seasonal temperature changes and labile carbon availability that control microbial activity (Hurley et al., 1995). An illustration of low microbial MeHg production at cold temperatures is the low MeHg relative to THg export summed for the world's largest Arctic rivers of 0.5% (Mu et al., 2019), compared to a global median of 2.2% (3.2% including particulate fluxes) (compiled from Table S1 in Bishop et al., 2020). However, MeHg production is highly site-specific, and Kirk and St. Louis (2009) found MeHg export near 10% of THg in two mesoscale Arctic rivers draining to Hudson Bay.

Hg methylation requires a labile carbon source. Windham-Myers et al. (2014) showed that microbial Hg methylation more than doubled in vegetated versus non-vegetated plots, attributing the increase in part to the presence of labile root exudates. We did not measure DOM lability in this study, but 10%-20% of the fluorescence in most samples was from C5 + C6 components, which are classically described as proteinlike (Fellman et al., 2010), suggesting that labile DOM was likely available for Hg methylation. Humic DOM provides substrate for Hg methylating bacteria (Zhao et al., 2017) but the large size of the Hg-DOM complex inhibits passage across the cell membrane (Hsu-Kim et al., 2013; Jiang et al., 2018). The stronger link of MeHg to humic-like fluorescence rather than protein-like fluorescence in this study suggests that the DOM involved in MeHg formation is different from the DOM involved in MeHg transport. In this catchment, MeHg was both transport- and supply-limited. MeHg was lowest in the coldest base flow period sampled (November; Figure 4), and unlike THg, MeHg was not elevated during snowmelt, suggesting supply limitation. Demers et al. (2010) also invoked supply-limitation, attributing an early snowmelt MeHg peak to flushing of the limited MeHg produced under the snowpack. MeHg was elevated during the October high-flow event, though to a lesser extent than THg, suggesting that the high flow promoted flushing of MeHg produced over the warm growing season, a sign of transport limitation. However, the MeHg peak early on the October hydrograph also suggests supply limitation. The muted MeHg response to our two high-flow events and positive loading on the temperature-dominated PC2 axis in the PCA support supply limitation.

Although MeHg was highest during the October storm, MeHg/THg fell to \sim 1% (as during snowmelt) at all sites (Figure 3d). Higher MeHg/THg ratios indicate that MeHg supply kept pace with transport at base flow, but supply rapidly depleted during storms. Our hypothesis 2, that MeHg would be most strongly associated with protein-like DOM, as found by Noh et al. (2018) in lakes, was refuted. A possible explanation is that Hg methylation and MeHg transport are

decoupled, and humic DOM was simply the carrier for MeHg that formed in association with protein-like (labile) DOM.

4.5 | Comparison to other studies

Authors that have linked Hg to DOM quality have usually focused on the DOM absorbance spectrum, and its derivative indices such as spectral slope and SUVA (UV₂₅₄/DOC; e.g., Burns et al., 2013). Those studies that have related Hg to DOM fluorescence metrics have typically linked Hg behaviour to the conventional Coble fluorescence peaks (C, A, etc.; Jiang et al., 2018), or derived fluorescence indices such as HIX, FI, and BI, which is similar to freshness index (Lescord et al., 2018). For example, in a lake with a mix of terrestrial and autochthonous DOM in China, Jiang et al. (2018) found that THg related poorly to bulk DOC, but significantly to the humic-like A and C and protein-like T and B peaks (all r values between 0.3 and 0.5, p < 0.05). These relations were much weaker than comparable ones (r > 0.9) in the present, all-terrestrial study. As in the present study, however, Jiang et al. (2018) found that MeHg related more weakly than THg to these fluorescence markers.

We identified only a few other field studies that applied PARAFAC to relate Hg behaviour to specific DOM components. Similar to the present study, Lescord et al. (2018) found that four humic-like PARAFAC components made up more than 80% of the fluorescent DOM at 47 river and lake sites in the forested boreal Attawapiskat basin in northern Ontario. A multiparameter model that tested seven PARAFAC components and six optical indices predicted THg with an r^2 of 0.72 and MeHg with an r^2 of 0.47 (Lescord et al., 2018). These models had much lower predictive power than OM components in the present study, but they outperformed DOC, which illustrates that deconvolution of DOM into fluorescence components clearly had high value for THg and MeHg prediction in this more diverse environment.

De Bonville et al. (2020), working in an aquatic system with recently constructed reservoirs in boreal Canada, found strong correlations of THg to humic DOM isolated from PARAFAC, but MeHg related poorly to all fluorescence components. In Utah's Provo River, Packer et al. (2020) noted that stream THg generally tracked the humic-like PARAFAC components, which dominated stream DOM. In contrast, Cárdenas et al. (2018) found that THg correlated most strongly with protein-like DOM components in as area of volcanic-sourced Hg in Patagonia. Noh et al. (2018) found MeHg distribution was linked with protein-like fractions of DOM in reservoirs. Schartup et al. (2015), seeking the source of DOM associated with Hg methylation in the ocean, used PARAFAC to differentiate terrestrial from marine DOM. Wang et al. (2022) did not apply PARAFAC, but found that Hg had the greatest affinity for humic, aromatic DOM.

5 | CONCLUSIONS

At a small forested Vermont catchment, we investigated the role of DOM quality in total mercury (THg) and methylmercury (MeHg)

dynamics in streamwater in spatial campaigns under five contrasting seasonal and hydrologic conditions. Isolation of DOM fluorescence components by a PARAFAC analysis indicated strong association of THg and MeHg with humic-like DOM fluorescence. Over a large range of DOC concentration and across seasons, THg tracked humic-like DOM components strongly (r > 0.94), but no single DOM component nor any combination were stronger predictors of THg than bulk DOC and UV absorbance at 254 nm (r = 0.957 in both cases), a simple indicator of aromaticity. THg correlated less strongly with the two protein-like DOM components, which comprised 10%-20% of FDOM. THg also had less robust relations with the conventional DOM quality metrihumification index (HIX), freshness index, fluorescence index (FI), and spectral slope ratio (SR), though THg had a strong negative correlation with FI over a large October storm hydrograph.

MeHg was weakly correlated to THg but had stronger seasonal variation. We hypothesized that MeHg would associate with the labile protein-like DOM components most conducive to methylation, but like THg, MeHg associated more strongly with humic-like than protein-like DOM. MeHg relations to DOM components mirrored those of THg, but were weaker across the board. Though protein-like DOM is more likely to facilitate methylation, humic DOM plays a larger role in its transport. Deconvolution of DOM into its fluorescence components shows promise for predicting and understanding stream THg and MeHg, but its application is most suited to diverse, mixed land-use landscapes.

ACKNOWLEDGEMENTS

This research was supported by a grant to VFT from the USGS Water Resources Research Institutes 104g programme, which also provided supplementary funds to USGS. Sleepers River Research Watershed is supported by the USGS Program. KAR was supported by an NSF GSP Fellowship. The authors thank Keith Kantack for field and laboratory assistance. Any use of trade, firm, or product names is for descriptive purposes only and does not imply endorsement by the U.S. Government.

DATA AVAILABILITY STATEMENT

Flow data presented in Figure 2, and flow and water temperature summarized in Table 1 are available in Shanley, Chalmers, et al. (2021) at https://doi.org/10.5066/P929KMVK. The mercury and other chemical data, including fluorescence and other optical data, are available in Shanley, Ryan, et al. (2021) at https://doi.org/10.5066/P9FP8SCV

ORCID

James B. Shanley https://orcid.org/0000-0002-4234-3437

REFERENCES

Aiken, G. R., McKnight, D. M., Thorn, K. A., & Thurman, E. M. (1992). Isolation of hydrophilic organic acids from water using nonionic macroporous resins. *Organic Geochemistry*, 18, 567–573.

Bigham, G. N., Murray, K. J., Masue-Slowey, Y., & Henry, E. A. (2017). Biogeochemical controls on methylmercury in soils and sediments:

- Implications for site management. Integrated Environmental Assessment and Management, 13(2), 249–263.
- Bishop, K., Lee, Y. H., Pettersson, C., & Allard, B. (1995). Methylmercury output from the Svartberget Catchment in northern Sweden during spring flood. *Water*, *Air*, *and Soil Pollution*, *80*(1), 445–454.
- Bishop, K., Shanley, J. B., Riscassi, A., de Wit, H. A., Eklöf, K., Meng, B., Mitchell, C., Osterwalder, S., Schuster, P. F., Webster, J., & Zhu, W. (2020). Recent advances in understanding and measurement of mercury in the environment: Terrestrial Hg cycling. Science of the Total Environment, 721, 137647. https://doi.org/10.1016/j.scitotenv.2020. 137647
- Branfireun, B. A., Cosio, C., Poulain, A. J., Riise, G., & Bravo, A. G. (2020). Mercury cycling in freshwater systems-an updated conceptual model. Science of the Total Environment, 745, 140906.
- Branfireun, B. A., & Roulet, N. T. (2002). Controls on the fate and transport of methylmercury in a boreal headwater catchment, northwestern Ontario, Canada. *Hydrology and Earth System Sciences*, 6(4), 785–794.
- Bravo, A. G., Bouchet, S., Tolu, J., Bjorn, E., Mateos-Rivera, A., & Bertilsson, S. (2017). Molecular composition of organic matter controls methylmercury formation in boreal lakes. *Nature Communications*, 8, 1–9
- Bravo, A. G., Kothawala, D. N., Attermeyer, K., Tessier, E., Bodmer, P., Ledesma, J. L., Audet, J., Casas-Ruiz, J. P., Catalán, N., Cauvy-Fraunié, S, & Colls, M. (2018). The interplay between total mercury, methylmercury and dissolved organic matter in fluvial systems: A latitudinal study across Europe. Water Research, 144, 172–182.
- Brigham, M. E., Wentz, D. A., Aiken, G. R., & Krabbenhoft, D. P. (2009). Mercury cycling in stream ecosystems. 1. Water column chemistry and transport. *Environmental Science & Technology*, 43(8), 2720–2725.
- Bro, R. (1997). PARAFAC. Tutorial and applications. Chemometrics and Intelligent Laboratory Systems, 38(2), 149-171.
- Burns, D. A., Aiken, G. R., Bradley, P. M., Journey, C. A., & Schelker, J. (2013). Specific ultra-violet absorbance as an indicator of mercury sources in an Adirondack River Basin. *Biogeochemistry*, 113, 451–466.
- Burns, D. A., Woodruff, L. G., Bradley, P. M., & Cannon, W. F. (2014). Mercury in the soil of two contrasting watersheds in the eastern United States. *PLoS One*, *9*(2), e86855.
- Bushey, J. T., Driscoll, C. T., Mitchell, M. J., Selvendiran, P., & Montesdeoca, M. R. (2008). Mercury transport in response to storm events from a northern forest landscape. *Hydrological Processes*, 22, 4813–4826. https://doi.org/10.1002/hyp.7091
- Cárdenas, C. S., del Carmen Diéguez, M., Queimaliños, C., Rizzo, A., Fajon, V., Kotnik, J., Horvat, M., & Guevara, S. R. (2018). Mercury in a stream-lake network of Andean Patagonia (Southern Volcanic Zone): Partitioning and interaction with dissolved organic matter. Chemosphere, 197, 262–270.
- Chen, H., Johnston, R. C., Mann, B. F., Chu, R. K., Tolic, N., Parks, J. M., & Gu, B. (2017). Identification of mercury and dissolved organic matter complexes using ultrahigh resolution mass spectrometry. *Environmental Science & Technology Letters*, 4(2), 59–65.
- Chen, J. B., Hintelmann, H., Zheng, W., Feng, X. B., Cai, H. M., Wang, Z. H., Yuan, S., & Wang, Z. (2016). Isotopic evidence for distinct sources of mercury in lake waters and sediments. *Chemical Geology*, 426, 33–44. https://doi.org/10.1016/j.chemgeo.2016.01.030
- Chiasson-Gould, S. A., Blais, J. M., & Poulain, A. J. (2014). Dissolved organic matter kinetically controls mercury bioavailability to bacteria. *Environmental Science & Technology*, 48(6), 3153–3161.
- Coble, P. G. (1996). Characterization of marine and terrestrial DOM in seawater using excitation-emission matrix spectroscopy. *Marine Chemistry*, 51(4), 325–346.
- Creed, I. F., Sanford, S. E., Beall, F. D., Molot, L. A., & Dillon, P. J. (2003). Cryptic wetlands: Integrating hidden wetlands in regression models of the export of dissolved organic carbon from forested landscapes. Hydrological Processes, 17(18), 3629–3648.

- De Bonville, J., Amyot, M., del Giorgio, P., Tremblay, A., Bilodeau, F., Ponton, D. E., & Lapierre, J. F. (2020). Mobilization and transformation of mercury across a dammed boreal river are linked to carbon processing and hydrology. *Water Resources Research*, *56*(10), e2020WR027951
- Demers, J. D., Driscoll, C. T., & Shanley, J. B. (2010). Mercury mobilization and episodic stream acidification during snowmelt: Role of hydrologic flow paths, source areas, and supply of dissolved organic carbon. Water Resources Research, 46, W01511. doi:10.1029/2008WR007021.
- Demers, J. D., Yavitt, J. B., Driscoll, C. T., & Montesdeoca, M. R. (2013). Legacy mercury and stoichiometry with C, N, and S in soil, pore water, and stream water across the upland-wetland interface: The influence of hydrogeologic setting. *Journal of Geophysical Research: Biogeosciences*, 118(2), 825–841.
- Dittman, J. A., Shanley, J. B., Driscoll, C. T., Aiken, G. R., Chalmers, A. T., & Towse, J. E. (2009). Ultraviolet absorbance as a proxy for total dissolved mercury in streams. *Environmental Pollution*, 157, 1953–1956.
- Dittman, J. A., Shanley, J. B., Driscoll, C. T., Aiken, G. R., Chalmers, A. T., Towse, J. E., & Selvendiran, P. (2010). Mercury dynamics in relation to dissolved organic carbon concentration and quality during high flow events in three northeastern US streams. Water Resources Research, 46(7), W07522. doi:10.1029/2009WR008351.
- Driscoll, C. T., Han, Y. J., Chen, C. Y., Evers, D. C., Lambert, K. F., Holsen, T. M., Kamman, N. C., & Munson, R. K. (2007). Mercury contamination in forest and freshwater ecosystems in the northeastern United States. *Bioscience*, 57(1), 17–28.
- Eagles-Smith, C. A., Silbergeld, E. K., Basu, N., Bustamante, P., Diaz-Barriga, F., Hopkins, W. A., Kidd, K. A., & Nyland, J. F. (2018). Modulators of mercury risk to wildlife and humans in the context of rapid global change. *Ambio*, 47(2), 170–197.
- Fellman, J. B., Hood, E., & Spencer, R. G. (2010). Fluorescence spectroscopy opens new windows into dissolved organic matter dynamics in freshwater ecosystems: A review. *Limnology and Oceanography*, 55(6), 2452–2462. https://doi.org/10.4319/lo.2010.55.6.2452
- Fitzgerald, W. F., & Clarkson, T. W. (1991). Mercury and monomethylmercury: Present and future concerns. Environmental health perspectives, 96, 159–166.
- Gilmour, C. C., Henry, E. A., & Mitchell, R. (1992). Sulfate stimulation of mercury methylation in freshwater sediments. *Environmental Science & Technology*, 26(11), 2281–2287.
- Gilmour, C. C., Podar, M., Bullock, A. L., Graham, A. M., Brown, S. D., Somenahally, A. C., Johs, A., Hurt, R. A., Bailey, K. L., & Elias, D. A. (2013). Mercury methylation by novel microorganisms from new environments. *Environmental Science & Technology*, 47, 11810–11820.
- Graham, A. M., Aiken, G. R., & Gilmour, C. C. (2013). Effect of dissolved organic matter source and character on microbial Hg methylation in Hg-S-DOM solutions. *Environmental Science & Technology*, 47(11), 5746-5754.
- Haitzer, M., Aiken, G. R., & Ryan, J. N. (2003). Binding of mercury (II) to aquatic humic substances: Influence of pH and source of humic substances. *Environmental Science & Technology*, 37(11), 2436–2441.
- Hansen, A. M., Kraus, T. E., Pellerin, B. A., Fleck, J. A., Downing, B. D., & Bergamaschi, B. A. (2016). Optical properties of dissolved organic matter (DOM): Effects of biological and photolytic degradation. *Limnology & Oceanography*, 61(3), 1015–1032.
- He, M., Tian, L., Braaten, H. F. V., Wu, Q., Luo, J., Cai, L. M., Meng, J. H., & Lin, Y. (2019). Mercury-organic matter interactions in soils and sediments: Angel or devil? *Bulletin of Environmental Contamination & Toxi*cology, 102(5), 621–627.
- Helms, J. R., Stubbins, A., Ritchie, J. D., Minor, E. C., Kieber, D. J., & Mopper, K. (2008). Absorption spectral slopes and slope ratios as indicators of molecular weight, source, and photobleaching of chromophoric dissolved organic matter. *Limnology & Oceanography*, 53(3), 955–969.

SHANLEY ET AL. WILEY 15 of 17

- Herrero Ortega, S., Catalán, N., Björn, E., Gröntoft, H., Hilmarsson, T. G.,
 Bertilsson, S., Wu, P., Bishop, K., Levanoni, O., & Bravo, A. G. (2018).
 High methylmercury formation in ponds fueled by fresh humic and algal derived organic matter. *Limnology & Oceanography*, 63(S1), S44–S53
- Hsu-Kim, H., Kucharzyk, K. H., Zhang, T., & Deshusses, M. A. (2013). Mechanisms regulating mercury bioavailability for methylating microorganisms in the aquatic environment: A critical review. *Environmental Science & Technology*, 47(6), 2441–2456.
- Hu, C., Muller-Karger, F. E., & Zepp, R. G. (2002). Absorbance, absorption coefficient, and apparent quantum yield: A comment on common ambiguity in the use of these optical concepts. *Limnology & Oceanogra*phy, 47(4), 1261–1267.
- Huguet, A., Vacher, L., Relexans, S., Saubusse, S., Froidefond, J. M., & Parlanti, E. (2009). Properties of fluorescent dissolved organic matter in the Gironde Estuary. *Organic Geochemistry*, 40(6), 706–719.
- Hurley, J. P., Benoit, J. M., Babiartz, C. L., Schafer, M. M., Andren, A. W., Sullivan, J. R., Hammond, R., & Webb, D. A. (1995). Influences of watershed characteristics on mercury levels in Wisconsin rivers. Environmental Science & Technology, 29, 1867–1875.
- Jiang, T., Chen, X., Wang, D., Liang, J., Bai, W., Zhang, C., Wang, Q., & Wei, S. (2018). Dynamics of dissolved organic matter (DOM) in a typical inland lake of the Three Gorges Reservoir area: Fluorescent properties and their implications for dissolved mercury species. *Journal of Environmental Management*, 206, 418–429.
- Jiskra, M., Saile, D., Wiederhold, J. G., Bourdon, B., Bjorn, E., & Kretzschmar, R. (2014). Kinetics of Hg(II) exchange between organic ligands, goethite, and natural organic matter studied with an enriched stable isotope approach. Environmental Science & Technology, 48, 13207–13217.
- Jiskra, M., Wiederhold, J. G., Skyllberg, U., Kronberg, R.-M., & Kretzschmar, R. (2017). Source tracing of natural organic matter bound mercury in boreal forest runoff with mercury stable isotopes. Environmental Science-Processes & Impacts, 19, 1235–1248.
- Kirk, J. L., & St. Louis, V. L. (2009). Multiyear total and methyl mercury exports from two major sub-Arctic rivers draining into Hudson Bay, Canada. Environmental Science & Technology, 43(7), 2254–2261.
- Kothawala, D. N., Murphy, K. R., Stedmon, C. A., Weyhenmeyer, G. A., & Tranvik, L. J. (2013). Inner filter correction of dissolved organic matter fluorescence. *Limnology & Oceanography: Methods*, 11(12), 616–630.
- Krabbenhoft, D. P., Branfireun, B. A., & Heyes, A. (2005). Biogeochemical, cycles affecting the speciation, fate and transport of mercury in the environment. In M. B. Parsons & L. J. B. Perciva (Eds.), Mercury: Sources, measurements, cycles, and effects. (short course series) (Vol. 34, pp. 139–156). Mineralogical Association of Canada.
- Krabbenhoft, D. P., Wiener, J. G., Brumbaugh, W. G., Olson, M. L., DeWild, J. F., & Sabin, T. J. (1999). A national pilot study of mercury contamination of aquatic ecosystems along multiple gradients. In D. W. Morganwalp, & H. T. Buxton (Eds.), U.S. Geological Survey Toxic Substances Hydrology Program: Proceedings of the Technical Meeting (Vol. 2, pp. 147–160). Charleston.
- Kronberg, R.-M., Drott, A., Jiskra, M., Wiederhold, J. G., Björn, E., & Skyllberg, U. (2016). Forest harvest contribution to boreal freshwater methyl mercury load. Global Biogeochemical Cycles, 30(6), 825–843.
- Lavoie, R. A., Amyot, M., & Lapierre, J.-F. (2019). Global meta-analysis on the relationship between mercury and dissolved organic carbon in freshwater environments. *Journal of Geophysical Research: Biogeosciences*, 124, 1508–1523. https://doi.org/10.1029/2018JG004896
- Lawaetz, A. J., & Stedmon, C. A. (2009). Fluorescence intensity calibration using the Raman scatter peak of water. Applied Spectroscopy, 63(8), 936–940.
- Lescord, G. L., Emilson, E. J. S., Johnston, T. A., Branfireun, B. A., & Gunn, J. M. (2018). Optical properties of dissolved organic matter and their relation to mercury concentrations in water and biota across a

- remote freshwater drainage basin. Environmental Science & Technology, 52, 3344–3353.
- Levanoni, O., Bishop, K., McKie, B. G., Hartman, G., Eklof, K., & Ecke, F. (2015). Impact of beaver pond colonization history on methylmercury concentrations in surface water. *Environmental Science & Technology*, 49, 12679-12687.
- Liem-Nguyen, V., Skyllberg, U., & Björn, E. (2017). Thermodynamic modeling of the solubility and chemical speciation of mercury and methylmercury driven by organic thiols and micromolar sulfide concentrations in boreal wetland soils. *Environmental Science & Technology*, 51(7), 3678–3686.
- Lyon, B. F., Ambrose, R., Rice, G., & Maxwell, C. J. (1997). Calculation of soil-water and benthic sediment partition coefficients for mercury. *Chemosphere*, 35(4), 791–808.
- Marvin-DiPasquale, M., Lutz, M. A., Brigham, M. E., Krabbenhoft, D. P., Aiken, G. R., Orem, W. H., & Hall, B. D. (2009). Mercury cycling in stream ecosystems. 2. Benthic methylmercury production and bed sediment—pore water partitioning. *Environmental Science & Technology*, 43(8), 2726–2732.
- McKnight, D. M., Boyer, E. W., Westerhoff, P. K., Doran, P. T., Kulbe, T., & Andersen, D. T. (2001). Spectrofluorometric characterization of dissolved organic matter for indication of precursor organic material and aromaticity. *Limnology & Oceanography*, 46(1), 38–48.
- Mierle, G., & Ingram, R. (1991). The role of humic substances in the mobilization of mercury from watersheds. *Water Air & Soil Pollution*, 56(1), 349–357.
- Mu, C., Zhang, F., Chen, X., Ge, S., Mu, M., Jia, L., Wu, Q., & Zhang, T. (2019). Carbon and mercury export from the Arctic rivers and response to permafrost degradation. Water Research, 161, 54–60.
- Murphy, K. R., Stedmon, C. A., Graeber, D., & Bro, R. (2013). Fluorescence spectroscopy and multi-way techniques. PARAFAC. Analytical Methods, 5(23), 6557–6566.
- Murphy, K. R., Stedmon, C. A., Wenig, P., & Bro, R. (2014). OpenFluor– An online spectral library of auto-fluorescence by organic compounds in the environment. *Analytical Methods*, 6(3), 658–661.
- Navrátil, T., Shanley, J. B., Rohovec, J., Dobešová, I., Matoušková, S., Roll, M., Nováková, T., & Oulehle, F. (2022). Mercury cycling during acid rain recovery at the forested Lesní Potok catchment, Czech Republic. *Hydrological Processes*, 35(6), e14255.
- Navrátil, T., Shanley, J. B., Rohovec, J., Hojdová, M., Penižek, V., & Buchtová, J. (2014). Distribution and pools of mercury in Czech forest soils. Water, Air, & Soil Pollution, 225, 1829. https://doi.org/10.1007/s11270-013-1829-1
- Noh, S., Kim, J., Hur, J., Hong, Y., & Han, S. (2018). Potential contributions of dissolved organic matter to monomethylmercury distributions in temperate reservoirs as revealed by fluorescence spectroscopy. *Environmental Science & Pollution Research*, 25(7), 6474–6486.
- Obrist, D., Johnson, D. W., & Lindberg, S. E. (2009). Mercury concentrations and pools in four Sierra Nevada forest sites, and relationships to organic carbon and nitrogen. *Biogeosciences Discussions*, *6*(1), 765–777.
- Obrist, D., Johnson, D. W., Lindberg, S. E., Luo, Y., Hararuk, O., Bracho, R., Battles, J. J., Dail, D. B., Edmonds, R. L., Monson, R. K., & Ollinger, S. V. (2011). Mercury distribution across 14 US forests. Part I: Spatial patterns of concentrations in biomass, litter, and soils. *Environmental Science & Technology*, 45(9), 3974–3981.
- Ohno, T. (2002). Fluorescence inner-filtering correction for determining the humification index of dissolved organic matter. *Environmental Science & Technology*, 36(4), 742–746.
- Packer, B. N., Carling, G. T., Veverica, T. J., Russell, K. A., Nelson, S. T., & Aanderud, Z. T. (2020). Mercury and dissolved organic matter dynamics during snowmelt runoff in a montane watershed, Provo River, Utah, USA. Science of The Total Environment, 704, 135297. https://doi.org/10.1016/j.scitotenv.2019.135297

- Pucher, M., Wünsch, U., Weigelhofer, G., Murphy, K., Hein, T., & Graeber, D. (2019). staRdom: Versatile software for analyzing spectroscopic data of dissolved organic matter in R. Water, 11(11), 2366.
- Ravichandran, M. (2004). Interactions between hg and dissolved organic matter review. *Chemosphere*, 55(3), 319–331.
- Rea, A. W., Lindberg, S. E., Scherbatskoy, T., & Keeler, G. J. (2002). Mercury accumulation in foliage over time in two northern mixed-hardwood forests. Water, Air, & Soil Pollution, 133(1-4), 49-67.
- Rimmer, C. C., Lloyd, J. D., McFarland, K. P., Evers, D. C., & Lane, O. P. (2019). Patterns of blood mercury variation in two long-distance migratory thrushes on. Ecotoxicology.
- Riscassi, A. L., & Scanlon, T. M. (2011). Controls on stream water dissolved mercury in three mid-Appalachian forested headwater catchments. Water Resources Research, 47, W12512. doi:10.1029/20 11WR010977.
- Risch, M. R., DeWild, J. F., Gay, D. A., Zhang, L., Boyer, E. W., & Krabbenhoft, D. P. (2017). Atmospheric mercury deposition to forests in the eastern USA. *Environmental Pollution*, 228, 8–18.
- Rodenhouse, N. L., Lowe, W. H., Gebauer, R. L., McFarland, K. P., & Bank, M. S. (2019). Mercury bioaccumulation in temperate forest food webs associated with headwater streams. Science of the Total Environment, 665, 1125–1134.
- Schartup, A. T., Ndu, U., Balcom, P. H., Mason, R. P., & Sunderland, E. M. (2015). Contrasting effects of marine and terrestrially derived dissolved organic matter on mercury speciation and bioavailability in seawater. *Environmental Science & Technology*, 49(10), 5965–5972.
- Schelker, J., Burns, D. A., Weiler, M., & Laudon, H. (2011). Hydrological mobilization of mercury and dissolved organic carbon in a snow-dominated, forested watershed: Conceptualization and modeling. *Journal of Geophysical Research - Biogeosciences*, 116, G1. https://doi.org/10. 1029/2010jg001330
- Schuster, P. F., Shanley, J. B., Marvin-Dipasquale, M., Reddy, M. M., Aiken, G. R., & Roth, D. A. (2008). Mercury and organic carbon dynamics during runoff episodes from a northeastern USA watershed. Water Air & Soil Pollution, 187, 89–108.
- Schwesig, D., & Matzner, E. (2001). Dynamics of mercury and methylmercury in forest floor and runoff of a forested watershed in Central Europe. *Biogeochemistry*, 53(2), 181–200.
- Sebestyen, S. D., Boyer, E. W., Shanley, J. B., Kendall, C., Doctor, D. H., Aiken, G. R., & Ohte, N. (2008). Sources, transformations, and hydrological processes that control stream nitrate and dissolved organic matter concentrations during snowmelt in an upland forest. Water Resources Research, 44, W12410.
- Shanley, J. B., & Bishop, K. (2012). Mercury cycling in terrestrial watersheds. In M. S. Bank (Ed.), Mercury in the environment: pattern and process (pp. 119–141). University of California Press.
- Shanley, J. B., Chalmers, A., Denner, J. C., Clark, S. W., Sebestyen, S. D., & Matt, S. (2022). Hydrology and biogeochemistry datasets from Sleepers River Research Watershed, Danville, Vermont, USA. *Hydrological Processes*, 36(2), e14495.
- Shanley, J. B., Chalmers, A. T., Denner, J. C., & Clark, S. F. (2021). Five-minute discharge; daily precipitation, stream runoff, and maximum and minimum air temperature; and annual precipitation and runoff for W-9 catchment, Sleepers River Research Watershed near Danville, Vermont, 1991–2018: U.S. Geological Survey data release, https://doi.org/10.5066/P929KMVK.
- Shanley, J. B., Krám, P., Hruska, J., & Bullen, T. D. (2004). A biogeochemical comparison of two well-buffered catchments with contrasting histories of acid deposition. Water, Air, & Soil Pollution: Focus, 4, 325–342.
- Shanley, J. B., Marvin-DiPasquale, M., Lane, O., Arendt, W., Hall, S., & McDowell, W. H. (2019). Resolving a paradox—High mercury deposition, but low bioaccumulation in northeastern Puerto Rico. *Ecotoxicology*, 29(8), 1207–1220.

- Shanley, J. B., Mast, M. A., Campbell, D. H., Aiken, G. R., Krabbenhoft, D. P., Hunt, R. J., Walker, J. F., Schuster, P. F., Chalmers, A., Aulenbach, B. T., Peters, N. E., Marvin-DiPasquale, M., Clow, D. W., & Shafer, M. M. (2008). Comparison of total mercury and methylmercury cycling at five sites using the small watershed approach. *Environmental Pollution*, 154, 143–154.
- Shanley, J. B., Ryan, K. A., Taylor, V. F., Chalmers, A. T., Perdrial, J., & Stubbins, A. (2021). Mercury, methylmercury, cations, dissolved organic carbon, and dissolved organic matter optical properties in small forest streams during five synoptic sampling campaigns at Sleepers River, Vermont, 2017–2018: U.S. Geological Survey data release, https://doi.org/10.5066/P9FP8SCV.
- Shanley, J. B., Schuster, P. F., Reddy, M. M., Roth, D. A., Taylor, H. E., & Aiken, G. R. (2002). Mercury on the move during snowmelt in Vermont. EOS, Transactions American Geophysical Union, 83(5), 45–48.
- Shanley, J. B., Sebestyen, S. D., McDonnell, J. J., McGlynn, B. L., & Dunne, T. (2015). Water's Way at Sleepers River watershed Revisiting flow generation in a post-glacial landscape, Vermont USA. Hydrological Processes, 29, 3447–3459.
- Skyllberg, U., Qian, J., Frech, W., Xia, K., & Bleam, W. F. (2003). Distribution of Hg, methyl Hg and organic sulphur species in soil, soil solution and stream of a boreal forest catchment. *Biogeochemistry*, *64*(1), 53–76.
- St. Louis, V. L., Rudd, J. W., Kelly, C. A., Hall, B. D., Rolfhus, K. R., Scott, K. J., Lindberg, S. E., & Dong, W. (2001). Importance of the forest canopy to fluxes of methyl mercury and total mercury to boreal ecosystems. *Environmental Science & Technology*, 35(15), 3089–3098.
- Stoken, O. M., Riscassi, A. L., & Scanlon, T. M. (2016). Association of dissolved mercury with dissolved organic carbon in US rivers and streams: The role of watershed soil organic carbon. *Water Resources Research*, 52(4), 3040–3051.
- Stubbins, A., Lapierre, J. F., Berggren, M., Prairie, Y. T., Dittmar, T., & del Giorgio, P. A. (2014). What's in an EEM? Molecular signatures associated with dissolved organic fluorescence in boreal Canada. *Environmental Science & Technology*, 48(18), 10598–10606.
- Tsui, M. T.-K., Liu, S., Brasso, R. L., Blum, J. D., Kwon, S. Y., Ulus, Y., Nollet, Y. H., Balogh, S. J., Eggert, S. L., & Finlay, J. C. (2019). Controls of methylmercury bioaccumulation in forest floor food webs. *Environ*mental Science & Technology, 53(5), 2434–2440.
- U.S. Environmental Protection Agency. (1999). Method 1631, revision B: Mercury in water by oxidation, purge and trap, and cold vapor atomic fluorescence. (pp. 1–33). Washington, D.C.: U.S. Environmental Protection Agency.
- Ullrich, S. M., Tanton, T. W., & Abdrashitova, S. A. (2001). Mercury in the aquatic environment: A review of factors affecting methylation. Critical Reviews in Environmental Science and Technology, 31(3), 241–293.
- Vermilyea, A. W., Nagorski, S. A., Lamborg, C. H., Hood, E. W., Scott, D., & Swarr, G. J. (2017). Continuous proxy measurements reveal large mercury fluxes from glacial and forested watersheds in Alaska. Science of the Total Environment, 599, 145–155.
- Vidon, P., Carleton, W., & Mitchell, M. J. (2014). Mercury proxies and mercury dynamics in a forested watershed of the US northeast. Environmental Monitoring and Assessment, 186(11), 7475–7488.
- Wagner, S., Fair, J. H., Matt, S., Hosen, J., Raymond, P., Saiers, J., Shanley, J. B., Dittmar, T., & Stubbins, A. (2019). Molecular hysteresis: Hydrologically-driven changes in riverine dissolved organic matter chemistry during a storm event. *Journal of Geophysical Research: Bio-geosciences*, 124(4), 759–774.
- Wang, Y., Liu, J., Liem-Nguyen, V., Tian, S., Zhang, S., Wang, D., & Jiang, T. (2022). Binding strength of mercury (II) to different dissolved organic matter: The roles of DOM properties and sources. Science of The Total Environment, 807, 150979.
- Watras, C. J., Bloom, N. S., Claas, S. A., Morrison, K. A., Gilmour, C. C., & Craig, S. R. (1995). Methylmercury production in the anoxic hypolimnion of a dimictic Seepage Lake. Water Air & Soil Pollution, 80, 735–745. https://doi.org/10.1007/BF01189725

- Weishaar, J. L., Aiken, G. R., Bergamaschi, B. A., Fram, M. S., Fujii, R, & Mopper, K. (2003). Evaluation of specific ultraviolet absorbance as an indicator of the chemical composition and reactivity of dissolved organic carbon. *Environmental Science & Technology*, 37(20), 4702–4708.
- Windham-Myers, L., Fleck, J. A., Ackerman, J. T., Marvin-DiPasquale, M., Stricker, C. A., Heim, W. A., Bachand, P. A., Eagles-Smith, C. A., Gill, G., Stephenson, M., & Alpers, C. N. (2014). Mercury cycling in agricultural and managed wetlands: A synthesis of methylmercury production, hydrologic export, and bioaccumulation from an integrated field study. Science of the Total Environment, 484, 221–231.
- Xu, J., Buck, M., Eklöf, K., Ahmed, O. O., Schaefer, J. K., Bishop, K., Skyllberg, U., Björn, E., Bertilsson, S., & Bravo, A. G. (2019). Mercury methylating microbial communities of boreal forest soils. *Scientific Reports*, 9(1), 1–13.
- Yamashita, Y., Kloeppel, B. D., Knoepp, J., Zausen, G. L., & Jaffé, R. (2011). Effects of watershed history on dissolved organic matter characteristics in headwater streams. *Ecosystems*, 14(7), 1110–1122. https://doi.org/10.1007/s10021-011-9469-z
- Zhao, L., Chen, H., Lu, X., Lin, H., Christensen, G. A., Pierce, E. M., & Gu, B. (2017). Contrasting effects of dissolved organic matter on mercury

- methylation by Geobacter sulfurreducens PCA and Desulfovibrio desulfuricans ND132. Environmental Science & Technology, 51(18), 10468–10475.
- Zsolnay, A., Baigar, E., Jimenez, M., Steinweg, B., & Saccomandi, F. (1999). Differentiating with fluorescence spectroscopy the sources of dissolved organic matter in soils subjected to drying. *Chemosphere*, 38(1), 45–50.

SUPPORTING INFORMATION

Additional supporting information may be found in the online version of the article at the publisher's website.

How to cite this article: Shanley, J. B., Taylor, V. F., Ryan, K. A., Chalmers, A. T., Perdrial, J., & Stubbins, A. (2022). Using dissolved organic matter fluorescence to predict total mercury and methylmercury in forested headwater streams, Sleepers River, Vermont USA. *Hydrological Processes*, *36*(5), e14572. https://doi.org/10.1002/hyp.14572